REPORT DOCUMENTATION PAGE

Form Approved
OMB No. 0704-0188

1. REPORT DATE *(DD-MM-YYYY)*	**2. REPORT TYPE**	**3. DATES COVERED** *(From - To)*
10/21/2010	Final Technical Report	04/01/2009-07/31/2010

4. TITLE AND SUBTITLE

Understanding Nanoscale Thermal Conduction and Mechanical Strength Correlation In High Temperature Ceramics With Improved Thermal Shock Resistance For Aerospace Applications

5a. CONTRACT NUMBER

5b. GRANT NUMBER
FA9550-09-1-0325

5c. PROGRAM ELEMENT NUMBER

6. AUTHOR(S)

Vikas Tomar and John E. Renaud

5d. PROJECT NUMBER

5e. TASK NUMBER

5f. WORK UNIT NUMBER

7. PERFORMING ORGANIZATION NAME(S) AND ADDRESS(ES)

University of Notre Dame du Lac, 511, Main Building, Notre Dame, IN-46556
and
Purdue University, 701 W Stadium Ave, West Lafayette, IN-47907

8. PERFORMING ORGANIZATION REPORT NUMBER

9. SPONSORING / MONITORING AGENCY NAME(S) AND ADDRESS(ES)

Air Force Office of Scientific Research, Program Manager: Dr. Kumar Jata

10. SPONSOR/MONITOR'S ACRONYM(S)

11. SPONSOR/MONITOR'S REPORT NUMBER(S)
AFRL-OSR-VA-TR-2012-0537

12. DISTRIBUTION / AVAILABILITY STATEMENT

Approved for Public Release

13. SUPPLEMENTARY NOTES

14. ABSTRACT

Ceramics and semiconductors are an integral part of today's energy devices. This research addresses conductive heat transfer issues in such materials using a combination of classical and quantum mechanical atomistic simulations. For any kind of thermal system, thermal stress and thermal conduction cannot be decoupled. Such analyses have to be performed together. This research also focuses on understanding how mechanical strength gets affected by thermal conduction and vice-versa. We have highlighted important role played by electronic thermal conductivity in overall thermal conduction across interfaces. This is the first time ever, quantum simulations of electronic and phononic thermal conductivity of any material system have been reported. We have performed first ever measurements of nanoscale and microscale high temperature creep in a ceramic. Such measurements could lead to significant advances in tunable thermal protection systems operating at temperatures ranging from very low to ultra-high. We have proven for the first time that materials with biomimetic phase morphology have thermal conductivity values independent of strain. This finding has strong implication for developing materials with thermal properties independent of applied stress.

15. SUBJECT TERMS

16. SECURITY CLASSIFICATION OF:			**17. LIMITATION OF ABSTRACT**	**18. NUMBER OF PAGES**	**19a. NAME OF RESPONSIBLE PERSON**
a. REPORT	**b. ABSTRACT**	**c. THIS PAGE**		15	Prof. Vikas Tomar
					19b. TELEPHONE NUMBER *(include area code)* +1-765-494-3423

Standard Form 298 (Rev. 8-98)
Prescribed by ANSI Std. Z39.18

Understanding Nanoscale Thermal Conduction and Mechanical Strength Correlation In High Temperature Ceramics With Improved Thermal Shock Resistance For Aerospace Applications

Final Technical Report

(April 01, 2009 to August 31, 2010)

Prepared By

Vikas Tomar, Ph.D.

Purdue University, West Lafayette, IN

John E. Renaud, Ph. D., P.E

University of Notre Dame, South Dend, IN

October 21, 2010

DoD Award Number: FA9550-09-1-0325

University of Notre Dame du Lac

511, Main Building

Notre Dame, IN-46556

Purdue University

701 W Stadium Ave

West Lafayette, IN-47907

DISCLAIMER

TABLE OF CONTENTS

EXECUTIVE SUMMARY

Ceramics and semiconductors are an integral part of today's energy devices. More often than not these materials consist of heterogeneities in the form of interfaces, grain boundaries, triple junctions, and second phase dispersion. These systems have to operate at very high thermal stress levels at very small length scales ranging from sub micrometers to supra-nanometers affecting device performance. This research addresses conductive heat transfer issues in such materials using a combination of classical and quantum mechanical atomistic simulations. For any kind of thermal system, thermal stress and thermal conduction cannot be decoupled. Such analyses have to be performed together. This research also focuses on understanding how mechanical strength gets affected by thermal conduction and vice-versa. The following are the main results:

1. We have highlighted important role played by electronic thermal conductivity in overall thermal conduction across interfaces, [1]. This is the first time ever, quantum simulations of electronic and phononic thermal conductivity of any material system have been reported.
2. We have performed first ever measurements of nanoscale and microscale high temperature creep in a ceramic, [2]. Such measurements could lead to significant advances in tunable thermal protection systems operating at temperatures ranging from very low to ultra-high.
3. We have proven for the first time that materials with biomimetic phase morphology have thermal conductivity values independent of strain, [3]. This finding has strong implication for developing materials with thermal properties independent of applied stress.
4. We have proven for the first time that that tensile straining and heat flow direction can be used to develop a thermal diode material from superlattice construction, [4, 5]. In addition, our group was the first to show that nanostructures with tunable thermal properties could be developed based on strain engineering, [5]. For this reason, the relevant publication was featured in the Virtual J. of Nanoscale Science and Technology (A collection of significant advances in nanotechnology).

Conference Publications:

1. Samvedi, V., and Tomar, V., 2011, A quantum mechanical study of the thermal conduction across a ZrB_2-SiC interface as a function of temperature and strain, Joint ASME-JSME International Heat Transfer Conference, paper number AJTEC2011-44643

International Journal Publications:

2. Gan, M, and Tomar, V., 2010, Role of length scale and temperature in indentation induced creep behavior of polymer derived Si-C-O ceramics, Materials Science and Engineering-A, vol 527, pp 7615-7623, DOI: 10.1016/j.msea.2010.08.016
3. Samvedi, V., and Tomar, V., 2010, Role of Straining and Morphology in Thermal Conductivity of a Set of Si-Ge Superlattices and Biomimetic Si-Ge Nanocomposites, J. Phys. D: Appl. Phys. 43 (2010) 135401 (11pp)
4. Samvedi, V, and Tomar, V., 2009, Role of interface thermal boundary resistance in overall thermal conductivity of Si-Ge multi-layered structures, Nanotechnology 20 (2009) 365701 (11pp) (Special Mention by Editors and Reviewers)
5. Samvedi, V, and Tomar, V., 2008, Role of heat flow direction, monolayer film thickness, and periodicity in controlling thermal conductivity of a Si-Ge superlattice system, *Journal of Applied Physics (featured in Virtual Journal of Nanoscale Science and Technology, volume 19, issue 4), vol 105, 013541*

DESCRIPTION OF RESEARCH WORK AND FINDINGS

This work focuses on understanding the correlation between heat transfer and interfacial construction in high temperature materials. Preliminary analyses have used classical molecular simulations and have shown that biomimetic interfacial arrangement results in a material where thermal conductivity is greatly insensitive to applied strains and moderate temperature variations. Based on these findings we have started quantum calculations to understand the role of interfacial phase change in heat transfer. The award was granted in April 2009 for a year. However, students started working on it in October-2009. This report presents work performed in the period since then. We have also started developing materials with different interfacial arrangements in our lab. In the following findings/status of classical molecular simulations is reported.

1. Findings from Classical Molecular Simulations:

A: Thermal Conduction is Superlattices

Superlattices are nanoscale engineered material system in which the thermal conduction properties could be tailored for applications such as high figure of merit (ZT) thermoelectric, microelectronics, and optoelectronics devices etc. [1] Widely researched superlattices such as $Si/Si_{1-x}Ge_x$, [2-4] GaAs/AlAs, [5] and Bi_2Te_3/Sb_2Te_3, [6] have been observed to have thermal conductivity values much lower than the bulk systems of similar composition. Factors that could be adjusted for tailoring the thermal conductivity of superlattices include the monolayer film thickness, periodicity, heat flow direction, straining, and temperature of operation. Different groups, [2,3], have worked on experimentally analyzing thermal transport in Si-Ge superlattice thin film structures as a function of the number of superlattice period and thickness. Chen and coworkers analyzed thermal conductivity in superlattice systems using numerical solutions of Boltzmann transport equations (BTE) and molecular dynamics (MD). [7-8] Chen and co-workers [9] performed MD simulations studying the dependence of thermal conductivity on the period length. NEMD analyses of Si-Ge superlattices with unspecified number of periods using Stillinger-Weber potential have been performed to study the dependence of thermal conductivity on the monolayer film thickness. [10,11]

Thus, analyses so far lack a combined account of factors such as tensile vs. compressive straining, change in number of periods, change in temperature, and change in the monolayer film thickness for a single superlattice material system. Recently, Zhou and coworkers [12] did an analysis of the effect of heat flow direction on thermal conductivity of composite metals. They found that the thermal properties change with the change in heat flow direction. The present work attempts to analyze the effect of tensile vs. compressive straining, change in number of periods, change in temperature, and change in the monolayer film thickness on the thermal conductivity of Si-Ge superlattices.

NON-EQUILIBRIUM MOLECULAR DYNAMICS

Figure 1 shows the simulation setup and the terminology for the superlattices analyzed in the presented research using NEMD. The simulation supercell is bounded by fixed atomic layers of length equivalent to 25Å, i.e. up to 9 atomic layers on either side, Fig. 1. In order to simulate a

thin film structure, PBCs are imposed in the directions transverse to the length of supercells. All layers have <100> orientation along the length of supercells. We chose 4x4 unit cells in transverse direction cross-sectional area [13]. As shown, a $(5_{Si}\times5_{Ge})_3$ structure represents an interfacial supercell of 5 nm thick Si thin film with 5 nm thick Ge thin film.

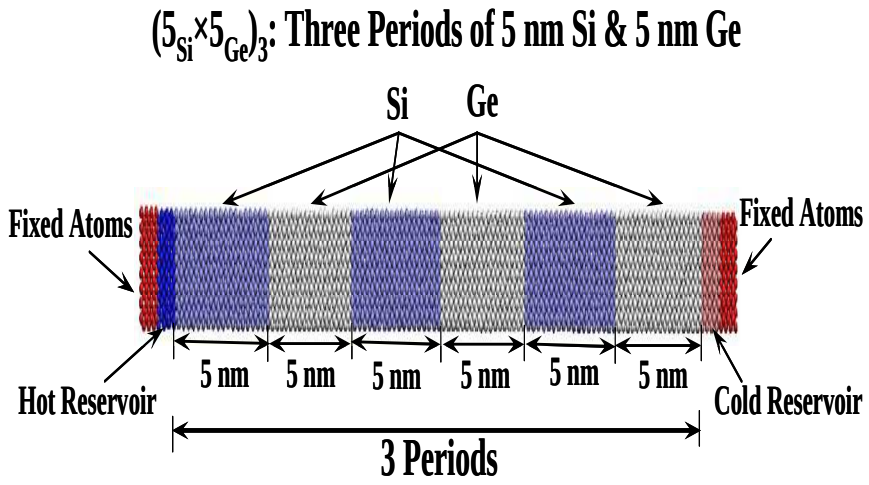

Figure 1: Terminology for layered structures

Subscript 3 denotes that the supercell consists of three periods. In the presented research, supercells with four different thicknesses (2.5nm, 5nm, 7.5nm, 10nm) and three different periods (1, 2, 3) are analyzed at three different temperatures (400 K, 600 K, and 800 K). We can calculate thermal conductivity, *k*, as

$$k = \frac{\Delta E_{hot} + \Delta E_{cold}}{t_s A |\nabla T|}. \tag{1}$$

Here, $\nabla T = (\Delta T / L)$ where ΔT is the temperature difference between the hot and cold reservoirs, *L* is the length of simulation cell, *A* is the cross-sectional area of the simulation supercell and t_s is the simulation time. To impose a constant heat flux, the hot and cold reservoirs need to be kept at a constant temperature. The energy supplied to the hot and cold reservoirs to maintain a constant temperature is based on momentum conservation scheme [14] and can be calculated from

$$\Delta E = \frac{1}{2}\sum_{i=1}^{N} m_i (v^2_{i,new} - v^2_{i,old}). \tag{2}$$

Here, $v_{i,old}$ is the old atomic velocity, $v_{i,new}$ is the new atomic velocity after scaling. In addition to computing *k*, thermal boundary resistance (TBR) across an interface *i*, R^i_{BD} can be calculated as

$$R^i_{BD} = (\Delta T_{\text{int}})_i / J, \tag{3}$$

$$J = \frac{1}{A}\frac{\sum_{j=1}^{n}\Delta E(j)}{t_s}. \qquad (4)$$

Here, ΔT_{int} represents the temperature drop measured at each interface and J gives the heat flux. To study the effect of strain on the thermal conductivity, we varied the strain by stretching the simulation cell from 10% to -10% with step size of 2% and ran MD simulation at each strain level to calculate the thermal conductivity.

Simulation Setup

The inter-atomic interactions for Si-Ge systems are described by the Tersoff bond-order potential [15]. During NEMD simulations to compute k at a temperature T, the superlattice system is equilibrated for 200 ps with a time step of 1 femtosecond (fs) in microcanonical (NVE) ensemble at temperature T. After equilibration, a temperature gradient is established by imposing $T_{hot}=T+30$ K and $T_{cold}=T-30$ K in the hot and the cold reservoir respectively using momentum conservation scheme[14], followed by further equilibration of the computational supercell for 500 ps. During this equilibration procedure, at each time step the values of k are calculated using Eq. (1). Calculations showed that the heat flux imposed on the superlattices by fixing up the hot and cold reservoir temperatures took approximately from 200 to 300 ps to get stabilized. For calculating temperature profile along the supercell length, each supercell was divided into thin slabs of length a little larger than both Si and Ge lattice constant. Once the values of k converge, the temperature profile along the length of the supercells is obtained by calculating average temperature of each slab based on the total kinetic energy of all atoms in the slab averaged over 100 ps.

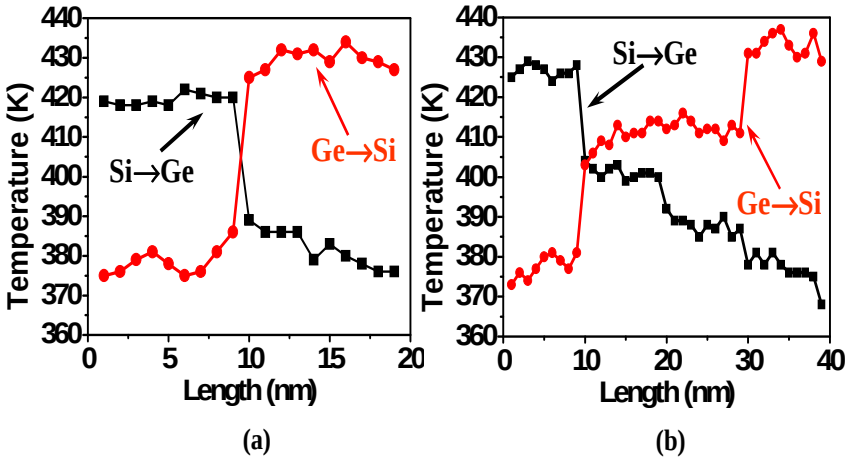

Figure 2: Temperature profile for (a) $(10_{si}\times10_{ge})_1$ and $(10_{ge}\times10_{si})_1$, and (b) $(10_{si}\times10_{ge})_2$ and $(10_{ge}\times10_{si})_2$ simulation systems

RESULTS

Figure 2 displays the temperature profile obtained along the length of the $(10_{Si}\times10_{Ge})_{x=1,\,2}$ and $(10_{Ge}\times10_{Si})_{x=1,\,2}$ simulation systems plotted for increasing period values. Fig. 2(a) shows temperature profile for $(10_{Si}\times10_{Ge})_1$ and $(10_{Ge}\times10_{Si})_1$ superlattices after convergence in k values corresponding to T=400 K. As shown in the curves in Fig. 2(a), a steep drop in temperature is observed at the interface of Si-Ge at the position corresponding to 10 nm. Such drop in the

temperature is attributed to the thermal boundary resistance offered by the interface and is observed to be different for the superlattice with different directions of heat current. This directional dependence is discussed later in section. Fig. 2 (b) shows the temperature drop across interfaces of $(10_{Si}\times10_{Ge})_2$ and $(10_{Ge}\times10_{Si})_2$ which also clearly shows the effect of interface boundary resistance. Another important aspect of interfacial conduction observed in Fig. 2 is the non-linear behavior of interfaces in offering resistance to heat flow as the number of interfaces increase. Calculations done on the basis of temperature drop recorded at each interface leads to the observation that the total TBR does not increase linearly with the increase in the number of interfaces, as suggested by Ref. [16].

Thermal Conductivity as a Function of Superlattice Period, Film Thickness, Temperature and Strain

We examined the variation of thermal conductivity of $(5_{Si}\times5_{Ge})_{1,2,\text{ and }3}$ and $(10_{Si}x10_{Ge})_{1,2,\text{ and }3}$ superlattices with increase in number of periods at temperatures 400K, 600K and 800K. Thermal conductivity increases with increase in monolayer thickness and with increase in number of periods. The rate of change of thermal conductivity with increase in the number of periods is found to be higher for thicker monolayer films. This is because, there are two factors competing with each other: (1) number of interfaces increase leading to higher cumulative R_{BD}, and (2) length of the superlattice system increase leading to a drop in the overall temperature gradient. For higher superlattice period thickness, i.e. with thicker monolayer films, the latter dominates over the former by a significant proportion. Accordingly, there is a steeper increase in the thermal conductivity value for higher period thickness.

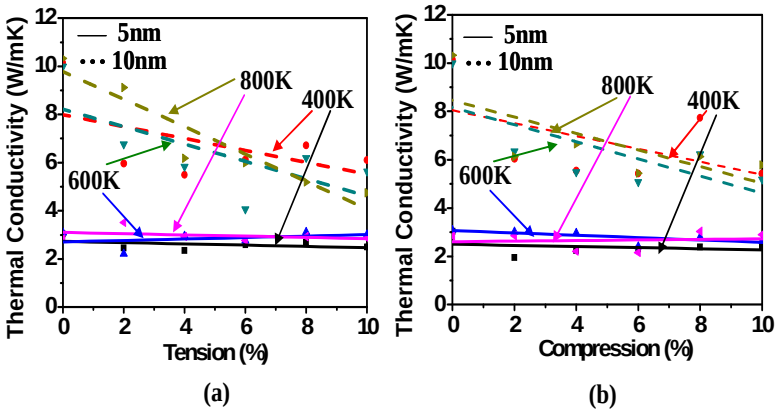

Figure 3: Thermal conductivity as a function of strain at different temperatures for $(5_{si}x5_{ge})_3$, $(10_{si}x10_{ge})_3$ structures

Effect of Straining on Thermal Conductivity as a Function of Temperature

Figure 3 displays the thermal conductivity of $(5_{Si}x5_{Ge})_3$ and $(10_{Si}x10_{Ge})_3$ systems as a function of temperature at different strain levels. Both compressive and tensile strain causes the thermal conductivity of superlattices to decrease. This trend is different from the earlier reported analyses in literature [16-18] regarding the effect of strain on the thermal conductivity. We conjecture that this difference is attributable to simulations being performed near or above Debye temperature values in our case. With the increase in the number of periods, the decrease in thermal conductivity is higher for higher strain and this trend is observed at all three

temperatures: 400K, 600K and 800K. It is observed that the straining has insignificant effect on the thermal conductivity of superlattices with 5 nm monolayer thickness, as we approach thin film limit.

Similarly, when tensile strain is applied, atomic distance increases, phonon relaxation time increases and structure stiffness decreases. But, an increase in the period thickness and periodicity causes the nucleation of structural defects[3] (identified as deviation from perfect single crystal structure). The formation of structural defects is more pronounced at high temperatures, which is experienced in this study.

The scattering at the defects and dislocations provide additional resistance to the flow of heat current through the material system, which leads to a reduction in the thermal conductivity with an increase in tensile strain.[16] It is also clear from the figures that the effect of straining is more pronounced at larger period thickness, which is again due to chances of dislocation nucleation being higher for higher period thickness. This decrease of thermal conductivity due to strain is seen to increase with an increase in the number of periods, at all period thicknesses.

Effect of Heat Flow Direction Reversal on Thermal Conductivity Values

Figure 4 shows a comparison of thermal conductivity as a function of temperature and heat flow direction for $(7.5_{Si}\times7.5_{Ge})_3$ and $(7.5_{Ge}\times7.5_{Si})_3$ superlattices, and for $(10_{Si}\times10_{Ge})_3$ and $(10_{Ge}\times10_{Si})_3$ superlattices. As shown, with an increase in the period thickness, the effect of the reversal in the heat flow direction becomes significant. This behavior can be attributed to the change in the frequency of the heat carrying phonons with the change in the heat flow direction.

For Si→Ge system, heat transfer characteristics are dominated by the phonons in Si monolayer whereas in Ge→Si, the heat transfer is determined by the phonons in Ge monolayer. Owing to a large atomic mass difference between Si and Ge, which reflects both in terms of large acoustic mismatch across Si-Ge layer and also in the difference in the frequency of Si and Ge phonons, the thermal resistance offered by an interface to a particular type of phonon varies. This difference grows with an increase in the number of periods and results in a larger drop in thermal conductivity value for Ge→Si system, when compared with Si→Ge system.

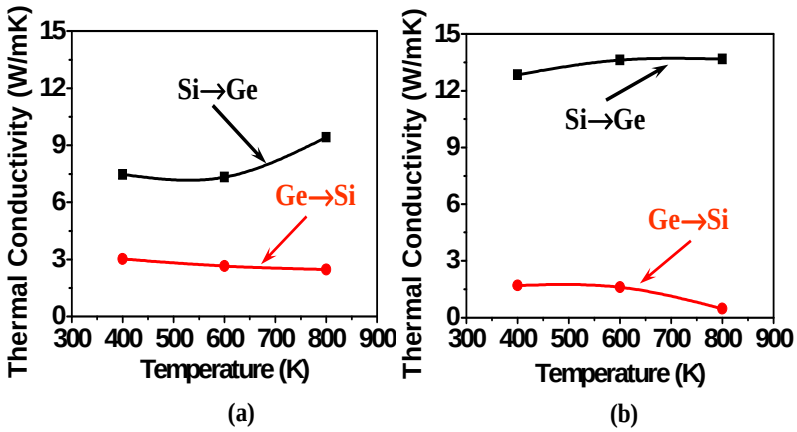

Figure 4: Dependence of thermal conductivity on heat flow direction as a function of temperature for (a) $(7.5_{si}\times7.5_{ge})_4$ and $(7.5_{ge}\times7.5_{si})_4$ superlattices, and (b) $(10_{si}\times10_{ge})_4$ and $(10_{ge}\times10_{si})_4$ superlattices

B: Thermal Conduction in Biomimetic Composites

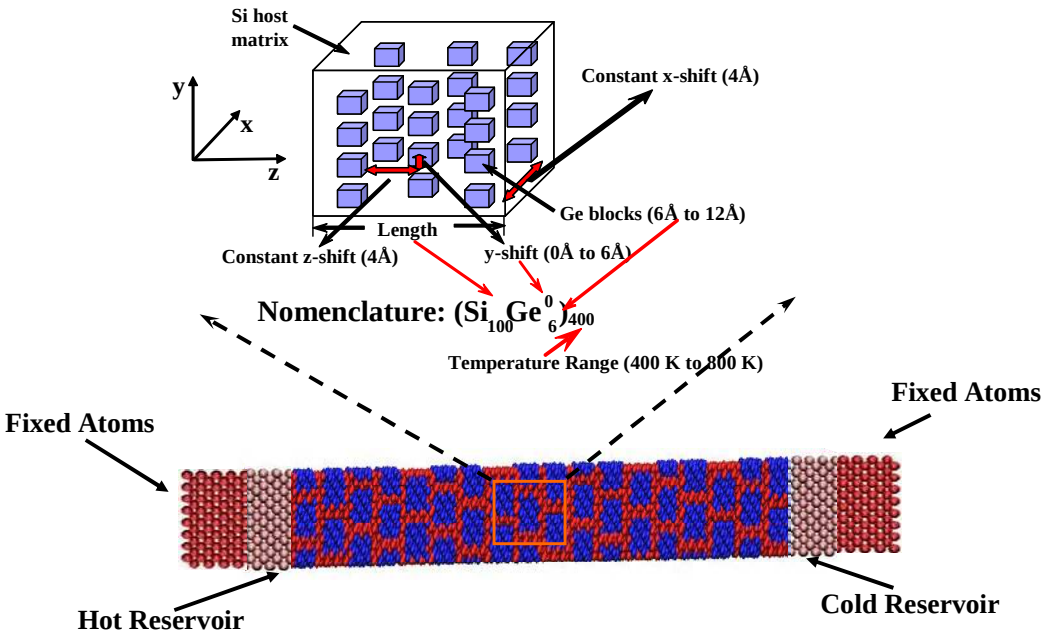

Figure 5 Simulation setup and terminology for the nanocomposite structures analyzed for thermal conduction. The staggered arrangement of Ge blocks inside Si host matrix is displayed along with various parameters considered in this study

The MD based thermal conductivity calculations in the case of biomimetic nanocomposites are based on the same framework used in the case of superlattices. Biomimetic nanocomposites with nanostructures in the form of nanoparticles and nanowires embedded in a host matrix material differ from conventional composite materials in their thermal and mechanical properties due to exceptionally high surface to volume ratio of the nanostructures acting as reinforcing phase. Atomistic analyses of the biomimetic nanocomposite thermal behavior are limited. Jeng and coworkers [19] have used Monte Carlo simulations to study the phonon transport and thermal conductivity reduction in the biomimetic nanocomposites with Si nanoparticle embedded in Ge host. Similar Monte Carlo analyses for the nanocomposites with Si tubular nanowires in Ge host have been performed by Yang and group [20]. In a recent work, Huang and group [21] have used molecular dynamics (MD) simulations to analyze similar systems as analyzed by Yang and group [20]. Yang and group [22] have theoretically studied phonon thermal conductivity of periodic two-dimensional nanocomposites with nanowires embedded in a host semiconductor material using phonon Boltzmann equation. They have concluded that the thermal conductivity of nanocomposites is always higher than that of a superlattice with the same characteristic thickness. The difference reduces as the dimensions of the two types of materials are reduced. A single conclusion common to all analyses has been that the reason behind biomimetic nanocomposites displaying low thermal conductivities is high percentage of atoms in the interfaces leading to significant phonon scattering. Interface atom fraction in the superlattices is usually lower than that in the biomimetic nanocomposites. Since structurally the superlattices and the biomimetic

nanocomposites are significantly different, their response to externally imposed mechanical straining should also be different. By a judicious combination of applied straining and morphology it should be possible to tailor the thermal conductivity of both types of materials. With this view, the present investigation focuses on understanding thermal behavior of a set of Si-Ge biomimetic nanocomposites using non-equilibrium molecular dynamics (NEMD) simulations at three different temperatures (400 K, 600 K, and 800 K) and at strain levels varying between -10% and 10%

Figure 5 displays the staggered arrangement of Ge blocks inside Si host matrix, highlighting various parameters that were varied to study their effect on the overall thermal conductivity of the biomimetic nanocomposites. The nomenclature $(Si_{100}Ge^{0}_{6})_{400}$ shown in the Fig. 5 helps in identifying each biomimetic nanocomposite analyzed. The subscript 100 on Si represents the thickness of the nanocomposite with Ge cubic blocks of size 6 Å as indicated by the Ge subscript of 6. The superscript 0 to Ge represents the Y-shift (extent to which a Ge particle is shifted in the y-direction with respect to an adjacent Ge particle). In the present work, nanocomposites with three different thicknesses: 10nm, 20nm and 30nm are analyzed. For each thickness, nanocomposites with three different Ge block sizes: 6 Å, 9 Å, and 12 Å are generated. Four values of Y-shift: 0 Å, 2 Å, 4 Å, and 6 Å are used for each nanocomposite thickness and for each Ge block size. It is made sure that all nanocomposites have equal number of Ge blocks at a cross-sectional view in the x-y plane. As shown in Fig. 5, the simulation supercell is bounded by fixed atomic layers of thickness equivalent to 25Å, i.e. up to 9 atomic layers on either side. Further increase in the thickness of fixed atomic layers did not change the presented results. Periodic boundary conditions (PBCs) are imposed in the directions transverse to the thickness of composite supercells to be able to simulate a thin film structure. Both, Si and Ge have <100> orientation along the thickness. A nanocomposite configuration may affect the lattice constant values of both Si and Ge. Based on the analyses by Volz and coworkers [23], lattice parameters for Si, a_{Si}=5.43 Å and for Ge, a_{Ge}=5.657 Å are used.

Effect of Straining as a Function of Temperature

Figure 6 displays the thermal conductivity variation of $Si_{100}Ge^{4}_{9}$ and $Si_{200}Ge^{4}_{9}$ nanocomposites as a function of tensile and compressive straining at three different temperatures: 400K, 600K and 800K. Variation of the thermal conductivity of the superlattices: $(5_{Si}x5_{Ge})_{1}$ and $(10_{Si}x10_{Ge})_{1,}$ [24], with comparable thickness has been plotted (dashed lines) along the nanocomposite thermal conductivity values in order to offer a comparison. As shown, a linear fit to the data on thermal conductivity for the nanocomposites as well as the superlattices can be obtained. It is observed that the straining has insignificant effect on the thermal conductivity of the nanocomposites with 10 nm thickness and slightly affects the thermal conductivity of the nanocomposites with 20 nm thickness. Overall, however, the thermal conductivity shows a stronger dependence on strain in the case of superlattices when compared to the nanocomposites, [24]. The superlattices with comparable thickness show an increase in thermal conductivity values as a function of tensile strain and decrease in the values as a function of compressive strain. This difference of the effect of straining on the thermal conductivity of nanocomposites when compared with superlattices can be explained from the phonon spectral density plots. In superlattice phonon spectrum, (not shown here, can be observed in our Journal of Physics Publication pointed out at first page), we have sharply defined peaks corresponding to certain frequencies which dominate the heat transfer. Correspondingly, only a limited frequencies are the most significant contributors to the heat transfer. On the contrary, in the nanocomposites there are no sharply defined peaks in the phonon spectrum. Accordingly, there is

a wide spectrum of phonon frequencies with equivalent spectral densities, which carry the heat current across.

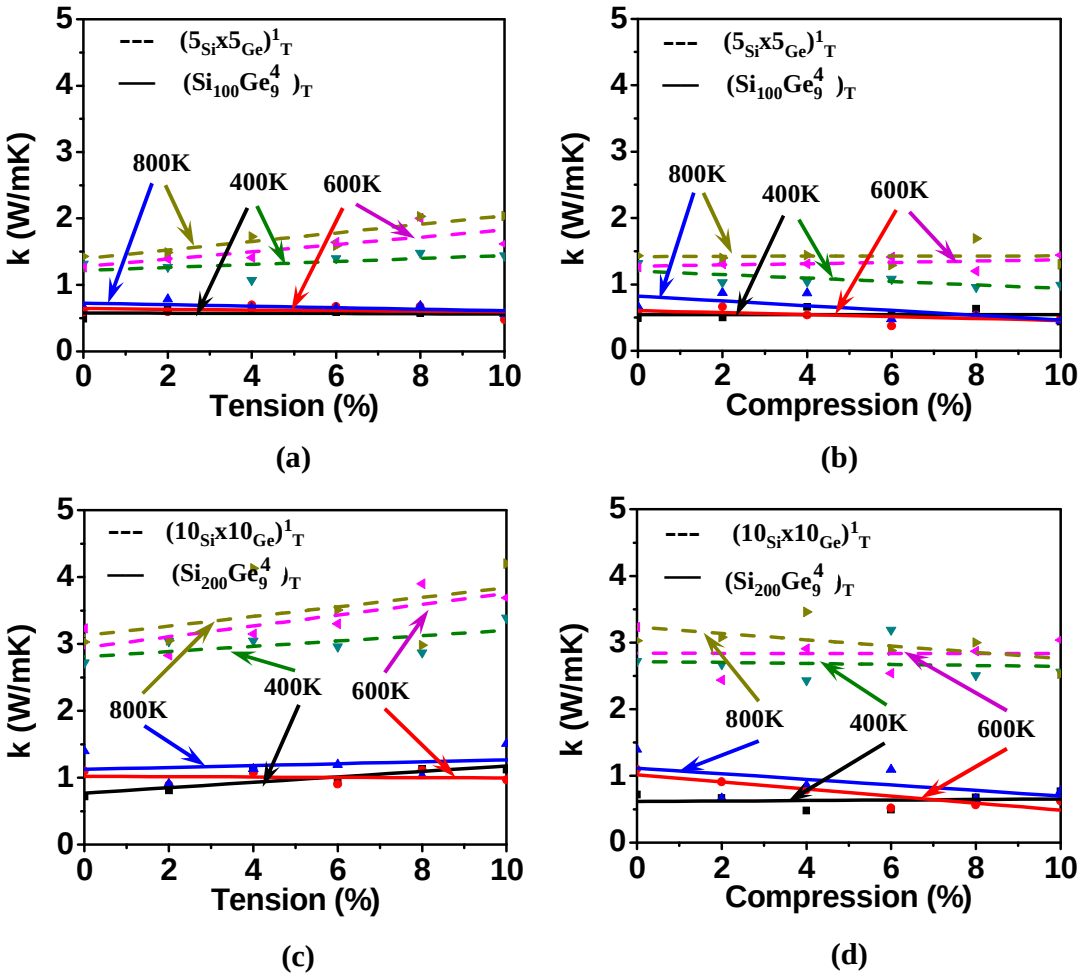

Figure 6 Comparisons of the thermal conductivity values of nanocomposites and superlattices of equal thickness as a function of strain. Plots are (**a)** for $Si_{100}Ge^4_9$ and $(5_{Si}x5_{Ge})_1$ under tension**, (b)** for $Si_{100}Ge^4_9$ and $(5_{Si}x5_{Ge})_1$ under compression, **(c)** for $Si_{200}Ge^4_9$ and $(10_{Si}x10_{Ge})_1$ under tension, and **(d)** for $Si_{200}Ge^4_9$ and $(10_{Si}x10_{Ge})_1$ under compression at 400 K, 600 K and 800 K.

Therefore, the reduction or increase in the interatomic distance caused by straining and the ensuing gain or loss in the stiffness, respectively, can affect superlattice phonon spectrum more owing to the dominance of a limited frequencies. In the nanocomposites, the effect is subdued, because the heat transfer is distributed across a much larger spectrum of wavelengths, Fig. 7. This difference of heat carrier phonons in the nanocomposites, when compared to those in superlattices leads to the observed difference in the variations of thermal conductivity shown in Fig. 6. To further explain the variation of thermal conductivity with straining, we can write *k* as, [16,18]

$$k = \frac{1}{3} C v^2 \tau_{ph} \quad \text{Or} \quad k = \frac{1}{3} C r_{ij}^{\,2} \frac{g}{m} \tau_{ph} . \tag{5}$$

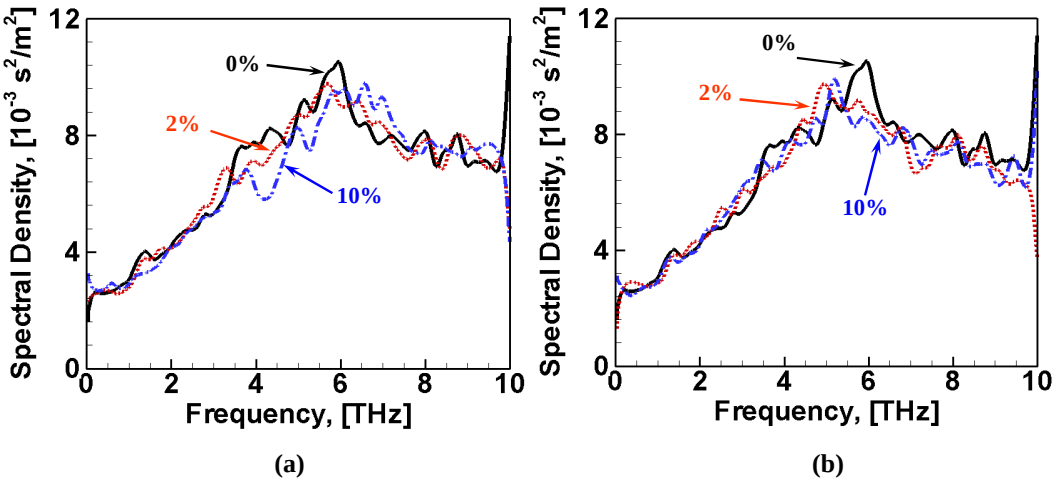

Figure 7 A comparison of the phonon spectral density at different strain levels for $Si_{100}Ge^{4}_{9}$ nanocomposite at 400 K, under **(a)** tension, and **(b)** compression

Here τ_{ph} gives phonon-phonon interaction or phonon relaxation time, g represents the stiffness constant of the atomic structure, and m gives the mass of atoms. In the above equation, the relations $l = v\tau_{ph}$ and $v = r_{ij}\sqrt{g/m}$ are used. Here, r_{ij} represents the average interatomic distance. From Eq. **Error! Reference source not found.** it can be shown that an increase in the compression causes a decrease in r_{ij} equivalently for both superlattices and nanocomposites.

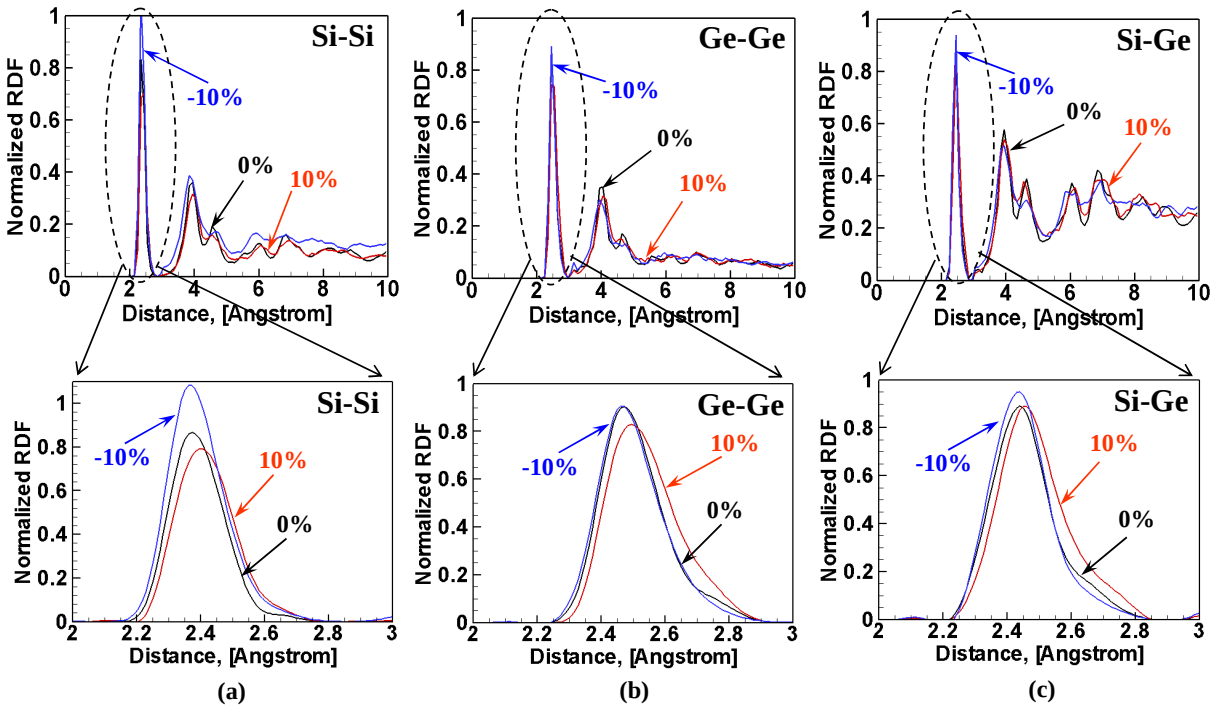

Figure 8 A comparison of the **(a)** Si-Si, **(b)** Ge-Ge, and **(c)** Si-Ge normalized radial distribution functions (RDF) at different strain levels for $Si_{100}Ge^{4}_{9}$ nanocomposite at 400 K

The reduction in the interatomic distance due to compression or increase in the interatomic distance due to tension significantly affects phonon relaxation time, τ_{ph}. Such changes in the interatomic distances also lead to the corresponding changes in the lattice stiffness. Since, nanocomposites have a significantly high interface atom fraction, the extent of r_{ij} reduction or increase with tension or compression, respectively, is limited when compared to that in superlattices, Fig. 8.

As shown in Fig. 8, the RDFs for the nanocomposites are not significantly affected by straining. Therefore, tension or compression affects superlattice thermal conductivity in a more significant manner. It is also clear from the Fig. 6 that the effect of straining is more pronounced at larger period thickness for superlattices and higher thickness nanocomposites, which can be attributed to chances of defect nucleation being higher for higher period thickness. In addition, for higher thickness nanocomposites, the interfacial atom fraction reduced when compared to that in smaller thickness nanocomposites (e.g. 10 nm here). This directly leads to higher effect of straining in higher thickness nanocomposites.

REFERENCES

[1] D. G. Cahill, W. K. Ford, K. E. Goodson, G. D. Mahan, A. Majumdar, H. J. Maris, R. Merlin, and S. R. Phillpot, J. Appl. Phys. **93,** 793 (2003).

[2] T. Borca-Tasciuc, W. Liu, J. Liu, Z. Taofang, D. W. Song, C. D. Moore, G. Chen, K. L. Wang, M. S. Goorsky, T. Radetic, R. Gronsky, T. Koga, and M. S. Dresselhaus, Superlattices and Microstructures **28,** 199-206 (2000).

[3] S.-M. Lee, D. G. Cahill, and R. Venkatasubramanian, Appl Phys. Lett. **70,** 2957-2959 (1997).

[4] S. T. Huxtable, A. R. Abramson, C.-L. Tien, A. Majumdar, C. LaBounty, X. Fan, G. Zeng, J. E. Bowers, A. Shakouri, and E. T. Croke, Appl Phys. Lett. **80** (2002).

[5] X. Y. Yu, G. Chen, A. Verma, and J. S. Smith, Appl Phys. Lett. **67** (1995).

[6] R. Venkatasubramanian, Phys. Rev. B **61,** 3091-3097 (2000).

[7] G. Chen and M. Neagu, Appl Phys. Lett. **71,** 2761-2763 (1997).

[8] S. Volz, J. B. Saulnier, G. Chen, and P. Beauchamp, Microelectronics Journal **31,** 815-819 (2000).

[9] Y. Chen, D. Li, J. R. Lukes, Z. Ni, and M. Chen, Physical Review B **72,** 1-6 (2005).

[10] E. S. Landry, A. J. H. Mcgauhey, and M. I. Hussein, Proceedings of HT2007 ASME-JSME Thermal engineering summer heat transfer conference (2007).

[11] S. Srinivasan and R. S. Miller, Num. Heat Transfer, Part B **52,** 297-321 (2007).

[12] Y. Zhou, B. Anglin, and A. Strachan, The Journal of Chemical Physics **127,** 1-11 (2007).

[13] P. K. Schelling, S. R. Phillpot, and P. Keblinski, Physical Review B **65,** 1-12 (2002).

[14] Z. Huang and Z. Tang, Physica B **373,** 291-296 (2006).

[15] J. Tersoff, Phys. Rev. B (Rapid Comm.) **39,** 5566-5568 (1989).

[16] A. R. Abramson, C.-L. Tien, and A. Majumdar, Journal of Heat Transfer **124,** 963-970 (2002).

[17] R. C. Picu, T. B. Tasciuc, and M. C. Pavel, Journal of Applied Physics **93,** 3535-3539 (2003).

[18] S. Bhowmick and V. B. Shenoy, The Journal of Chemical Physics **125** (2006).

[19] M.-S. Jeng, R. Yang, D. Song, and G. Chen, Journal of Heat Transfer **130,** 022410-1 (2008).

[20] R. Yang, G. Chen, and M. S. Dresselhaus, Phys. Rev. B **72** (2005).

[21] X. Huang, X. Huai, S. Liang, and X. Wang, J. Phys. D: Appl. Phys. **42,** 095416 (2009).

[22] R. Yang and G. Chen, Phys. Rev. B **69** (2004).

[23] S. Volz, J. B. Saulnier, G. Chen, and P. Beauchamp, Microelectronics J. **31,** 815-819 (2000).

[24] V. Samvedi and V. Tomar, Journal of Applied Physics **105** (2009).